JOINT INSTITUTE FOR NUCLEAR RESEARCH
Bogoliubov Laboratory of Theoretical Physics

FINAL REPORT OF THE SUMMER STUDENT PROGRAM

Weyl semi-metal junctions with unconventional superconducting coupling

Supervisor:
Dr. Moitri Maiti

Author:
Hidde Dijkstra,
Netherlands,
Université de Genève

Participation period:
July 8 – August 16

Dubna, 2019

Abstract

We study the transport properties of an inversion breaking Weyl semi-metal at the normal to super-conducting interface. Here the superconducting gap pairs electrons in a certain node to the opposite branch in its time reversal partner of the same chirality. We follow the paper of Zhang et al. [1] for singlet superconductivity and expand to triplet superconductivity. We have found that the location of the Weyl nodes in momentum space dominates the physics and results in the same behavior as for singlet pairing. We recommend repeating the calculations for the time reversal symmetry breaking Weyl semi-metal where the superconducting gap is zero at the nodes.

Acknowledgement

Contents

1 Introduction

We study the transport properties between a junction of a normal Weyl semi-metal (WSM) and a superconducting WSM. WSMs have special nodes in their band structure where momentum and spin are locked relatively to each other. At these nodes the dispersion is linear in three dimensions. As such the Hamiltonian shows clear resemblances to the Dirac Hamiltonian as found in graphene. Similarly to the two dimensional K points in graphene, Weyl nodes also come in pairs depending on the symmetries of the system. Weyl semi-metals discern themselves by having a non-degenerate band structure around the Weyl node, which requires three dimensions to achieve. Until a few years ago this state of matter was merely theory but has recently been discovered in tantalum phosphide [2] and tantalum arsenide [3]. We interest ourselves in how this locking interacts with the coupling of electrons with opposite spin and momentum in a WSM superconductor where superconductivity can be induced by proximity effect. We follow the paper of Zhang et al. [1] for singlet superconductivity and expand to triplet superconductivity.

2 Singlet junction

2.1 Time reversal symmetric Weyl semi-metal

A WSM is a topological phase of matter in three dimensions, where the non-degenerate conduction and valence band touch in certain points with a linear dispersion. When either inversion or time-reversal symmetry (TRS) is broken spin and momentum lock to form pairs of chiral Weyl nodes: one with spin and momentum in the same direction (positive chirality) and one with opposite direction (negative chirality). Breaking of either symmetry separates the pair in momentum space and as such protects them from local perturbations. We choose to break inversion symmetry and keep TRS which requires a node of a certain chirality to have a TRS partner of the same chirality and opposite momentum. The minimum number of nodes for inversion breaking is four, where the distinct chiralities are decoupled. We describe such a system with the low energy Hamiltonian [1]:

$$H(\mathbf{k}) = (k_x \mp \bar{k}_x)\sigma_x + k_y\sigma_y + (k_z \mp \bar{k}_z)\sigma_z, \tag{1}$$

with each combination of signs constituting a different Weyl node. Two identical signs indicate positive chirality while opposite signs negative. The nodes are at the zeros of energy: $\pm(\bar{k}_x, 0, \pm\bar{k}_z)$, see figure 1, with $k_F^2 = \bar{k}_x^2 + \bar{k}_z^2$ the Fermi wavevector at the Weyl node.
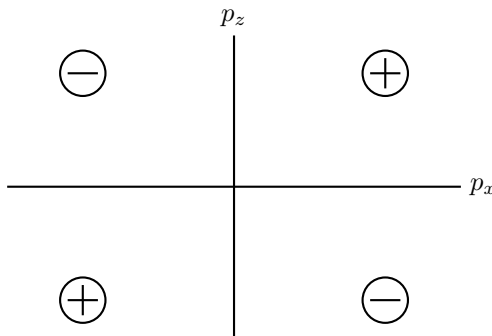

Figure 1: An inversion breaking Weyl semi-metal has four nodes at $\pm(\bar{k}_x, 0, \bar{k}_z)$, two of each chirality. TRS couples nodes of the same chirality, as such the minimal amount of nodes is four.

A WSM-superconductor is described by the Bogoliubov-de Gennes (BdG) Hamiltonian. We consider a junction with propagation along the z-axis: the WSM is in the normal state for $z < 0$ and in the superconducting state for $z > 0$. As such we wish to transform the Hamiltonian of equation 1 back to position space for use in the BdG Hamiltonian. A unitary transformation in real space allows us to move the dependence on these constants to the basis states. The basis states acquire a position dependent complex phase of $e^{\pm i\bar{k}_x x \pm i\bar{k}_z z}$. Additionally we include a chemical potential μ relative to the Weyl point to get the Hamiltonian for a Weyl node:

$$H' = \begin{pmatrix} -i\partial_z - \mu & k_\parallel e^{-i\theta} \\ k_\parallel e^{i\theta} & i\partial_z - \mu, \end{pmatrix} \tag{2}$$

in the basis $\Phi_{e,1} = (c_{1,\uparrow}, c_{1,\downarrow})^T$. Here we have assumed plane wave solutions in the x-y plane with transverse momentum $k_\parallel$ and azimuthal angle θ. The Fermi velocity and $\hbar$ are set to one so the wavevector and energy have the same units.

2.2 Singlet superconductivity

Now we consider how the Hamiltonian changes when we induce superconductivity (SC) for $z > 0$ by means of the proximity effect. The SC gap couples electrons with their time-reverse counterpart in the other Weyl node of the same chirality. The time reversed basis is the complex conjugate of the normal electron basis and has an opposite complex phase coming from $\bar{k}_x$ and $\bar{k}_z$. The contribution to the energy from the gap is proportional to the overlap between electron and time reversed wavefunctions of node i and j [1]:

$$\Delta E_{ij} \propto \frac{1}{\Omega} \int d\mathbf{r} \, \Phi_{h,i}^* \Phi_{e,j} = \frac{1}{\Omega} \int d\mathbf{r} \, e^{i\bar{k}_x(\sigma_{j,\bar{k}_x} + \sigma_{i,\bar{k}_x})x + i\bar{k}_z(\sigma_{j,\bar{k}_z} + \sigma_{i,\bar{k}_z})x}, \tag{3}$$

with $\sigma_{i,a}$ the sign of constant a with respect to node i. If the signs are not opposite for both constants the phases interfere destructively and the contribution to the energy is negligible for $\bar{k}_x L_x \gg 1$ and $\bar{k}_z L_z \gg 1$ with L_x and L_z the system dimensions in the x and z direction. As such electrons can only couple to the holes in the other Weyl node of the same chirality. The BdG Hamiltonian for the N-S interface now reduces to four blocks of identical form:

$$h_{\text{BdG}} = \begin{pmatrix} -i\partial_z - \mu(z) & k_\parallel e^{-i\theta} & \Delta(z) & 0 \\ k_\parallel e^{i\theta} & i\partial_z - \mu(z) & 0 & \Delta(z) \\ \Delta^*(z) & 0 & i\partial_z + \mu(z) & -k_\parallel e^{-i\theta} \\ 0 & \Delta^*(z) & -k_\parallel e^{i\theta} & -i\partial_z + \mu(z) \end{pmatrix}, \tag{4}$$

in the basis $\Phi(\mathbf{r}) = \begin{pmatrix} c_{1,\uparrow}(\mathbf{r}) & c_{1,\downarrow}(\mathbf{r}) & c_{2,\uparrow}^\dagger(\mathbf{r}) & -c_{2,\downarrow}^\dagger(\mathbf{r}) \end{pmatrix}^T$ and with $\Delta(z)$ the SC gap.

We now choose $\Delta(z) = \Delta_0 e^{i\phi}\Theta(z)$, with ϕ the superconducting phase, and $\mu(z) = \mu_N\Theta(-z) + \mu_S\Theta(z)$ with $\Delta_0 > 0$ and $\Theta(z)$ the Heaviside step function. The eigenstates of this Hamiltonian describe the particles involved in the scattering process at the interface between the normal WSM and the SC WSM. The eigenenergies are given as $\varepsilon = \pm\sqrt{|\Delta^2 + (|\mathbf{k}| \pm \mu)^2}$ with the first $\pm$ indicating the branch and the $\pm\mu$ the electron/hole-like nature of the particle.

2.3 Reflection and transmission

We restrict ourselves to the scattering of an incoming electron which can reflect as an electron or hole, or get transmitted as an electron/hole-like quasi-particle as shown in figure 2. The BTK model
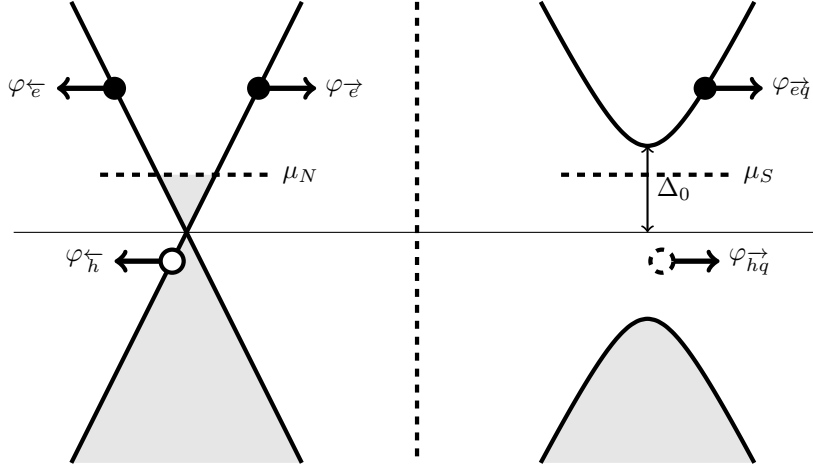
Figure 2: The scattering of an incoming electron $\varphi_{\vec{e}}$ at the interface with a SC. It can reflect as an electron $\varphi_{\overleftarrow{e}}$ or a hole $\varphi_{\overleftarrow{h}}$ or gets transmitted as a quasi-particle of electron-like $\varphi_{\overrightarrow{eq}}$ or hole-like $\varphi_{\overrightarrow{hq}}$ nature. Take note that the scattered holes belong to the other Weyl node of the same chirality.

[4] expresses the scattering process in terms of reflection coefficients a_0 (electron) and b_0 (hole) and transmission coefficients c_0 (electron-like) and d_0 (hole-like). The total wave equation is the sum of incoming and reflected wavefunctions in the normal region and transmitted wavefuctions in the superconducting region:

$$\Psi(z) = \begin{cases} \varphi_{\vec{e}}(z) + b_0 \varphi_{\overleftarrow{e}}(z) + a_0 \varphi_{\overleftarrow{h}}(z), & z < 0 \\ c_0 \varphi_{\overrightarrow{eq}}(z) + d_0 \varphi_{\overrightarrow{hq}}(z), & z > 0 \end{cases} \tag{5}$$

Here the arrows indicate the direction of the group velocity of the respective particles. The group velocity of a hole-like particle is the inverse of the one an electron-like particle would have in a similar state. The relevant wavefunctions in the normal region are:

$$\varphi_{\vec{e}}(z) = \begin{pmatrix} 1 & \kappa_e e^{i\theta_k} & 0 & 0 \end{pmatrix} e^{ik_e z}, \tag{6}$$

$$\varphi_{\overleftarrow{e}}(z) = \begin{pmatrix} \kappa_e e^{-i\theta_k} & 1 & 0 & 0 \end{pmatrix} e^{-ik_e z}, \tag{7}$$

$$\varphi_{\overrightarrow{h}}(z) = \begin{pmatrix} 0 & 0 & -\kappa_h e^{-i\theta_k} & 1 \end{pmatrix} e^{-ik_e z}, \tag{8}$$

$$\varphi_{\overleftarrow{h}}(z) = \begin{pmatrix} 0 & 0 & 1 & -\kappa_h e^{i\theta_k} \end{pmatrix} e^{ik_h z}, \tag{9}$$

with $k_{e(h)} = \text{sgn}(\mu_N \pm \varepsilon)\sqrt{(\mu_N \pm \varepsilon)^2 - k_\parallel^2}$ and $\kappa_{e(h)} = \pm(\mu_N \pm \varepsilon - k_{e(h)})/k_\parallel$. When $|\mu_N - \varepsilon| < k_\parallel$ a hole reflection is non-physical. Here we set $k_h = 0$ and $\kappa_h = 1$.

In the superconducting region the quasi-particle wavefunctions are:

$$\varphi_{\overrightarrow{eq}}(z) = \begin{pmatrix} 1 & \kappa_{eq} e^{i\theta_k} & e^{-i\beta - i\phi} & \kappa_{eq} e^{-i\beta - i\phi + i\theta_k} \end{pmatrix} e^{ik_{eq} z}, \tag{10}$$

$$\varphi_{\overleftarrow{eq}}(z) = \begin{pmatrix} \kappa_{eq} e^{i\theta_k} & 1 & \kappa_{eq} e^{-i\beta - i\phi - i\theta_k} & e^{-i\beta - i\phi} \end{pmatrix} e^{-ik_{eq} z}, \tag{11}$$

$$\varphi_{\overrightarrow{hq}}(z) = \begin{pmatrix} -\kappa_{hq} e^{-i\beta + i\phi - i\theta_k} & e^{-i\beta + i\phi} & -\kappa_{hq} e^{-i\theta_k} & 1 \end{pmatrix} e^{-ik_{hq} z}, \tag{12}$$

$$\varphi_{\overleftarrow{hq}}(z) = \begin{pmatrix} e^{-i\beta + i\phi} & -\kappa_{hq} e^{-i\beta + i\phi + i\theta_k} & 1 & -\kappa_{hq} e^{-i\theta_k} \end{pmatrix} e^{ik_{hq} z}, \tag{13}$$

3

with $k_{eq(hq)} = \text{sgn}(\mu_S \pm \text{Re}(\Omega))\sqrt{(\mu_S \pm \Omega)^2 - k_\parallel^2}$ and $\kappa_{eq(hq)} = \pm(\mu_S \pm \Omega - k_{eq(hq)})/k_\parallel$. For subgap energies $\varepsilon \leq \Delta_0$: $\beta = \arccos(\varepsilon/\Delta_0)$ and $\Omega = i\sqrt{\Delta_0^2 - \varepsilon^2}$, for supragap energies: $\varepsilon > \Delta_0$: $\beta = -i\text{arccosh}(\varepsilon/\Delta_0)$ and $\Omega = \text{sgn}(\varepsilon)\sqrt{\varepsilon^2 - \Delta_0^2}$. Note that for $\varepsilon \gg \Delta_0$ the transmitted wavefunctions tend to the ones we expect for a normal WSM.

The total wavefunction must satisfy continuity at the interface both of the probability current and the wavefunction itself. The former requires normalization of the individual particle wavefunctions with the respective particle group velocity. The latter uniquely defines the coefficients a_0, b_0, c_0, and d_0 (these are given in the appendix). The reflection and transmission coefficients are equal to the ratio of the normal components of the probability currents of the respective particle and the incident electron. Given f the normalized electron-like and g the normalized hole-like components of the wavefunction the probability current:

$$\overrightarrow{J}_P = \frac{1}{m}(\text{Im}(f^*\nabla f) - \text{Im}(g^*\nabla g)), \tag{14}$$

notice that the electron-like and hole-like wavefunctions contribute different signs.

The reflection and transmission coefficients are:

$$R_{eh} = \frac{|(\kappa_e^2 - 1)(\kappa_{hq}\kappa_{eq} + 1)|^2}{|\gamma|^2 \mathcal{Z}_h}|, \tag{15}$$

$$R_{ee} = |\gamma|^{-2}|e^{i\beta}(\kappa_h\kappa_{hq} - 1)(\kappa_e - \kappa_{eq}) - e^{-i\beta}(\kappa_h + \kappa_{eq})(\kappa_e\kappa_{hq} + 1)|^2, \tag{16}$$

$$T_{ee} = |1 - |e^{2i\beta}||\frac{|(\kappa_e^2 - 1)(\kappa_h\kappa_{hq} - 1)|^2}{|\gamma|^2 \mathcal{Z}_{eq}}, \tag{17}$$

$$T_{eh} = |1 - |e^{-2i\beta}||\frac{|(\kappa_e^2 - 1)(\kappa_{eq} + \kappa_h)|^2}{|\gamma|^2 \mathcal{Z}_{hq}}, \tag{18}$$

with

$$\gamma = (\kappa_e\kappa_{eq} - 1)(\kappa_h\kappa_{hq} - 1)e^{i\beta} + (\kappa_{hq} + \kappa_e)(\kappa_{eq} + \kappa_h)e^{-i\beta}, \tag{19}$$
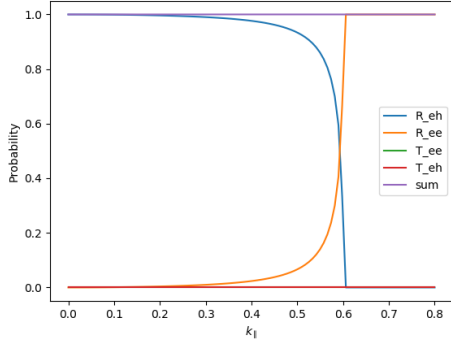
$$\mathcal{Z}_h = \left(\frac{1 + |\kappa_e|^2}{1 + |\kappa_h|^2}\right) \cdot \left|\frac{\varepsilon - \mu_N}{\varepsilon + \mu_N}\right| \cdot \left|\frac{k_e}{k_h}\right|, \tag{20}$$

$$\mathcal{Z}_{eq} = \left(\frac{1 + |\kappa_e|^2}{1 + |\kappa_{eq}|^2}\right) \cdot \left|\frac{\Omega + \mu_S}{\varepsilon + \mu_N}\right| \cdot \left|\frac{k_e}{k_{eq}}\right|, \tag{21}$$
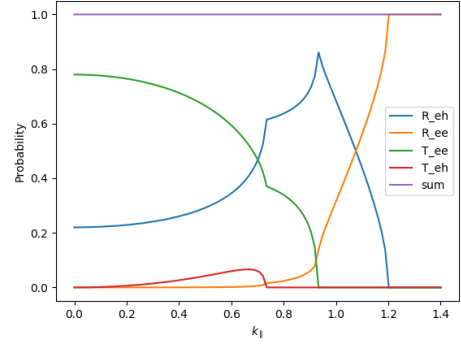
$$\mathcal{Z}_{hq} = \left(\frac{1 + |\kappa_e|^2}{1 + |\kappa_{hq}|^2}\right) \cdot \left|\frac{\Omega - \mu_S}{\varepsilon + \mu_N}\right| \cdot \left|\frac{k_e}{k_{hq}}\right|. \tag{22}$$

In figure 3 we plot examples of the behavior of the coefficients in the subgap and for the supragap at identical chemical potential for the normal WSM and the superconducting WSM.

(a) Subgap: $\varepsilon = 0.7\Delta_0$ with $\mu_N = \mu_S = 0.1\Delta_0$. There is no transmission possible so $R_{ee} + R_{eh} = 1$. For $k_\parallel \geq \varepsilon - \mu_N$ the holewavevector k_h becomes zero and we have only electron reflection: $R_{ee} = 1$.

(b) Supragap: $\varepsilon = 1.3\Delta_0$ with $\mu_N = \mu_S = 0.1\Delta_0$. Reflection of a hole is possible for $k_\parallel < \varepsilon - \mu_N$, transmission of electron-like particles is possible for $k_\parallel < \Omega + \mu_S$ and of hole-like particles for $k_\parallel < \Omega - \mu_S$.

Figure 3: The reflection and transmission coefficients in the sub- and supragap for identical chemical potential as a function of the transverse momentum $k_\parallel$. The sum of all four coefficients always equals one.

2.4   Differential conductance

The reflection coefficients define the relative current coming from an incoming electron with transverse momentum $\mathbf{k}_\parallel$ and charge e: if the electron passes the interface the relative current is one, if it reflects as an electron the net current is zero and if it reflects as a hole (transmits as a Cooper pair) the relative current is two. As such we give the normalized conductance as:

$$g_{NS} = \frac{1}{\pi(\mu_N + \varepsilon)^2} \int_A d\mathbf{k}_\parallel (1 - R_{ee} + R_{eh}), \tag{23}$$

which is the differential conductance dI/dV per channel. Here the integration area A is such that $|\mathbf{k}_\parallel| \leq |\mu_N + \varepsilon|$ since the kinetic energy of the particle cannot exceed the total particle energy. For singlet superconductivity we have rotational symmetry in the azimuthal angle and the integral reduces to 1d.

This integral leads to the same conductance plots, figure 4, and zero bias plot, figure 5, as found in the paper by Zhang [1] with non-equivalent formulas. We have however been able to reproduce the plots with the formulas in the paper on the condition that we add $\pi/2$ to the $\tilde{\alpha}_h$ given in the paper.
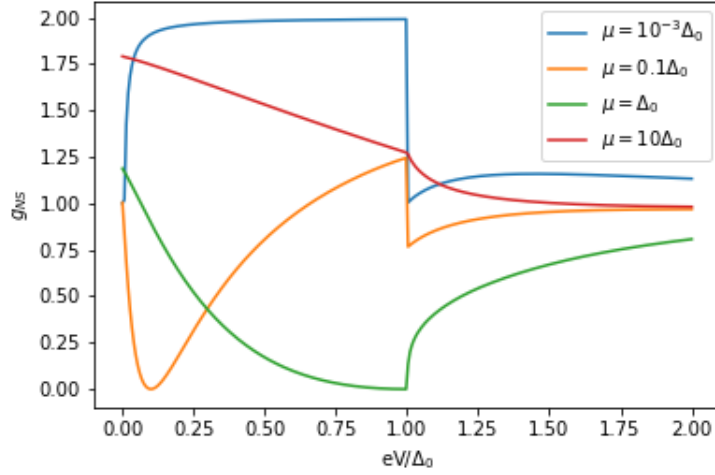
Figure 4: Normalized differential conductance for various values of $\mu_S = \mu_N$ as a function of the energy ε. When $\varepsilon = \mu < \Delta_0$ the conductance goes to zero as there is no hole state to reflect to. When $\varepsilon = \Delta_0$ transmission of particles becomes possible resulting in a discontinuity in the conductance. When $\mu \approx 0$ we have perfect Andreev reflection and a conductance of 2.
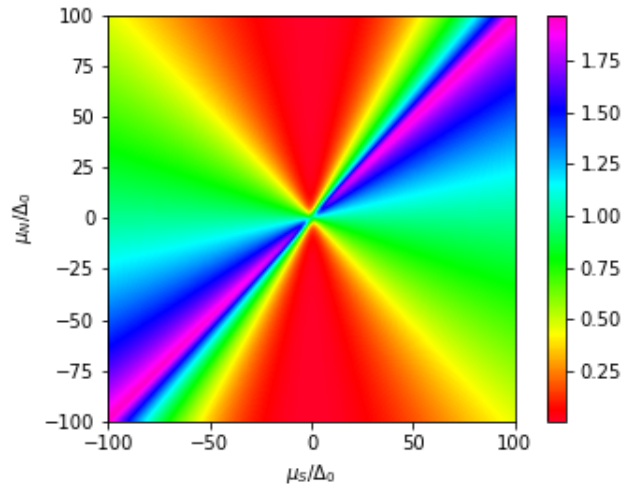

Figure 5: Normalized differential conductance at zero bias for various combinations of μ_N and μ_S. Maximal conductance occurs when the two chemical potentials are equal and perfect Andreev reflection result in normalized conductance of two.

3 Unconventional superconductivity

3.1 Triplet pairing for TRS-breaking WSM

We now wish to expand on the result of the paper by Zhang [1] by adding a momentum dependence to the superconducting gap Δ. Schnyder [5] describes the possibility of a Anderson-Brinkman-Morel (ABM) state in a Weyl semi-metal with triplet-wave pairing: $\Delta = \Delta_0(p_x + ip_y)/k_F$. Here p_x and p_y refer to the system momenta, while k_x and k_y refer to the linearized momenta around the Weyl nodes located at $(0, 0, \pm k_F)$ for a TRS breaking WSM. Schnyder gives the linearized BdG Hamiltonian of such a system as:

$$\mathcal{H}(\mathbf{k}) = h(\mathbf{k})\tau_z + \frac{\Delta_0}{k_F}\mathbf{k} \cdot (\hat{\mathbf{e}}_1\tau_x + \hat{\mathbf{e}}_2\tau_y), \tag{24}$$

with $h(\mathbf{k})$ the normal WSM dispersion and τ_i the Pauli matrices acting on particle-hole space. The eigenenergies of this Hamiltonian are $\varepsilon(\mathbf{k}) = \pm\sqrt{|h(\mathbf{k})|^2 + (\Delta_0/k_F)^2(k_x^2 + k_y^2)}$.

Here the triplet pairing is not able to gap out the Weyl nodes in the superconducting region since the gap is zero for $p_x = p_y = 0$. This in contrast to the BCS case we studied before where transmission of particles is suppressed below the gap.

3.2 Triplet pairing for inversion-breaking WSM

We now apply the ABM pairing to our inversion-breaking WSM. The triplet-pairing is non-zero at our Weyl nodes at $\pm(\bar{k}_x, 0, \pm\bar{k}_z)$ for non-zero $\bar{k}_x$ which is required for our argument for suppression of intraband coupling to hold ($\bar{k}_x L_x \gg 1$). In the low energy limit around the Weyl node the pairing becomes: $\Delta = \Delta_0(\bar{k}_x + k_\parallel e^{i\theta})/k_F$, breaking the azimuthal symmetry required to reduce the integral of the normalized conductance (23) to 1d. When $\bar{k}_x \gg k_\parallel$ we can neglect this symmetry breaking contribution and get the same conductance as before, albeit with the gap scaled by $\bar{k}_x/k_F$.

In fact this ratio times Δ_0 gives the relevant energy scale for the system. The interesting physics happens for energies ε of the order of the gap. The transverse momentum is however bounded by the energy of the incoming particle plus the chemical potential:

$$k_\parallel \lesssim \frac{|\bar{k}_x + k_\parallel e^{i\theta}|}{k_F}\Delta_0 + \mu_N. \tag{25}$$

Since $k_F \gg \mu_N, \Delta_0$ and $k_\parallel$ we state $k_\parallel \lesssim \bar{k}_x/k_F$: interesting ε are of the order of $\bar{k}_x/k_F$ in units of Δ_0. We take our effective gap $\bar{\Delta}_0$ to be $\Delta_0 \cdot \bar{k}_x/k_F$ while we keep our units in Δ_0.

For our theoretical model we set $k_F = 20$ and $\bar{k}_x = 4$ in units of the gap Δ_0. Realistically k_F should be significantly larger even for high values of T_c (and as such large values for Δ_0) but this drowns out the θ dependence. For instructive purposes we take these values to stay in a low energy limit ($\varepsilon \approx \bar{\Delta}_0 = k_F/100$) but still have visible results.
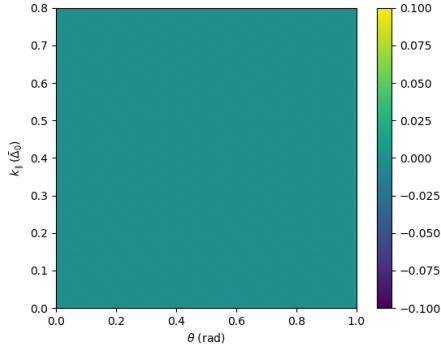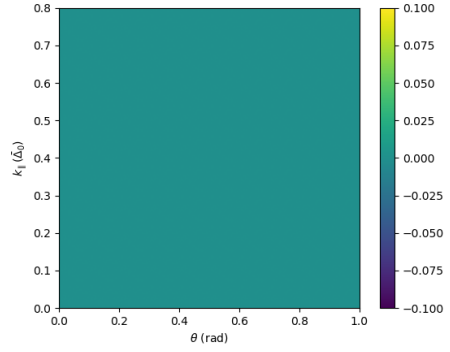
3.3 Reflection and transmission for triplet sub-gap
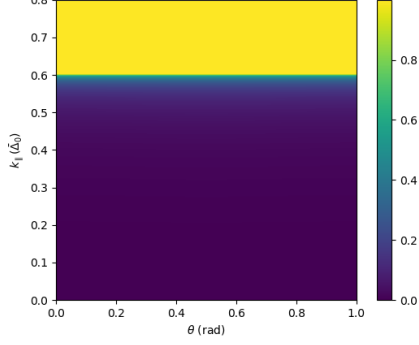
(a) Heatmap of R_{ee}, for $k_\parallel > \varepsilon - \mu_N$ all incoming electrons are reflected as electrons.
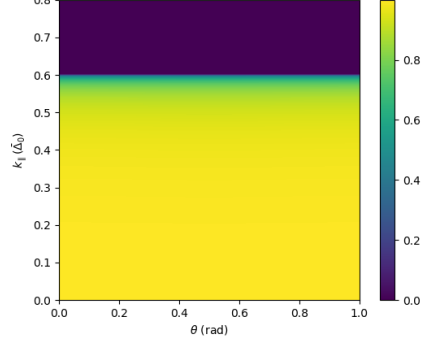
(b) Heatmap of R_{eh}, for $k_\parallel > \varepsilon - \mu_N$ there are no hole states with enough total momentum to support $k_\parallel$ and the probability of Andreev reflection goes to zero.

(c) Heatmap of T_{ee}, there is zero probability of transmission in the sub-gap.

(d) Heatmap of T_{eh}, there is zero probability of transmission in the sub-gap.

Figure 6: Reflection and transmission coefficients for triplet pairing at $\varepsilon = 0.7\bar{\Delta}_0$ and $\mu_N = \mu_S = 0.1\bar{\Delta}_0$, the effective sub-gap. Here the dependence of the gap on the azimuthal angle is negligible since the position of the cut-off does not rely on the value of the gap. These plots are equivalent to the ones in figure 3 with a scaled gap.
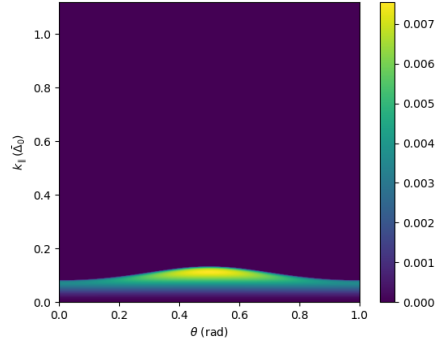
3.4 Reflection and transmission for triplet gap-edge
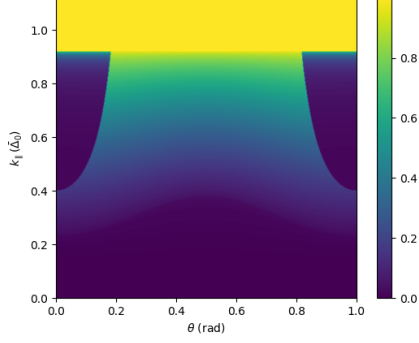
(a) Heatmap of R_{ee}, for $k_\parallel > \varepsilon - \mu_N$ all incoming electrons are reflected as electrons. For $\theta \approx 0$ a parabolic sub-gap region forms where the probability of reflecting as an electron goes to zero.
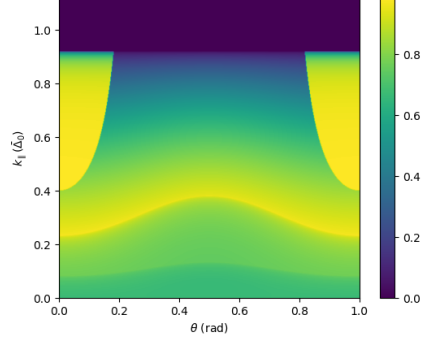
(b) Heatmap of R_{eh}, for $k_\parallel > \varepsilon - \mu_N$ Andreev reflection is impossible. For $\theta \approx 0$ a parabolic sub-gap region forms where Andreev reflection dominates. For θ around $1/2$ we are in the supra-gap with a probability spike when transmission of particles becomes impossible: $\varepsilon > \Omega + \mu_S$. Ω is close to zero here and is more sensitive to fluctuations of θ.
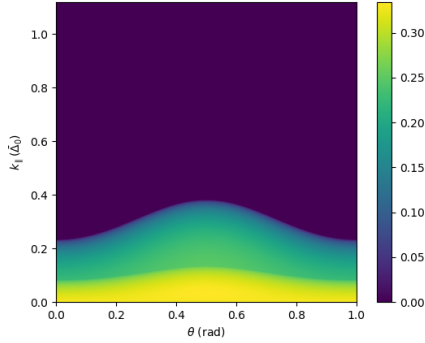

(c) Heatmap of T_{ee}, there are two "wave fronts", one for $\varepsilon = \Omega + \mu_S$ and one for $\varepsilon = \Omega - \mu_S$ with transmission more likely in the latter.


(d) Heatmap of T_{eh}, for $k_\parallel \lesssim \Omega - \mu_S$ transmission is most likely. The probability is however still below 0.01 so its contribution to conductivity is negligible.

Figure 7: Reflection and transmission coefficients for triplet pairing at $\varepsilon = 1.02\bar{\Delta}_0$ and $\mu_N = \mu_S = 0.1\bar{\Delta}_0$, just beyond the effective gap edge. Here the dependence of the gap on the azimuthal angle is the most pronounced since the value of θ decides whether a certain region is in the supra- or sub-gap.
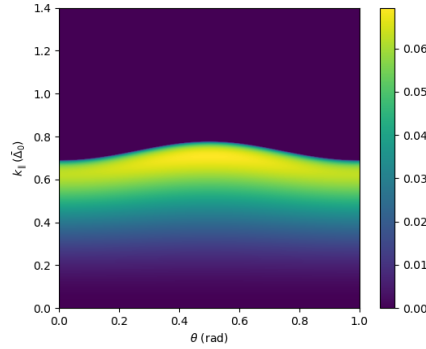
3.5 Reflection and transmission for triplet supra-gap
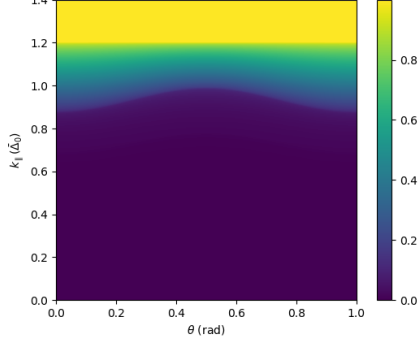
(a) Heatmap of R_{ee}, for $k_\parallel > \varepsilon - \mu_N$ all incoming electrons are reflected as electrons. This reflection becomes significant for $k_\parallel > \Omega + \mu_S$ as is also apparent for singlet pairing in figure 3b.
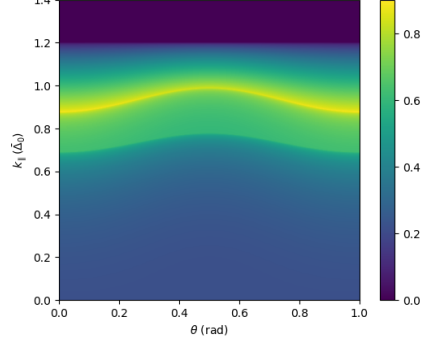
(b) Heatmap of R_{eh}, similarly as for the singlet pairing as in figure 3b we have a sharp peak in reflection probability for $k_\parallel = \Omega + \mu_S$ where we clearly see the sine-like behavior of the gap.
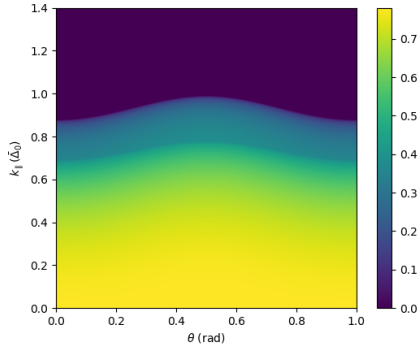
(c) Heatmap of T_{ee}, for small transverse momentum transmission of electrons dominates the scattering process.

(d) Heatmap of T_{eh}, a shifted version of the transmission of holes for $\varepsilon = 1.02\bar{\Delta}_0$ as in figure 7d but with higher probability.

Figure 8: Reflection and transmission coefficients for triplet pairing at $\varepsilon = 1.3\bar{\Delta}_0$ and $\mu_N = \mu_S = 0.1\bar{\Delta}_0$, in the effective supra-gap. Here the dependence of the gap on the azimuthal angle is clearly visible in the region $\Omega - \mu_S \lesssim k_\parallel \lesssim \Omega + \mu_S$. These plots coincide with those in figure 3b for singlet pairing with a scaled gap.

3.6 Triplet differential conductance

The triplet differential conductance is defined in the same way as the singlet differential conductance in equation (23). In figure 9 we see the triplet conductance for the equivalent values as in the singlet case, see figure 4. The behavior in the sub-gap and supra-gap are close to identical while at the gap-edge the conductance changes more smoothly. Accordingly there is no change to the zero-bias plot respective to figure 5 for the singlet since $\varepsilon = 0$ always lies in the sub-gap. Here the θ dependence is negligible as we have seen in the sub-gap triplet reflection and transmission plots (figure 6). As k_F becomes larger relative to the maximal gap Δ_0 the jump at the gap edge reduces in width. For $k_F > 100\Delta_0$ the difference between the triplet and singlet case becomes close to indistinguishable for the whole energy spectrum. The only real effect is scaling of the gap by the position of the Weyl node in momentum space.
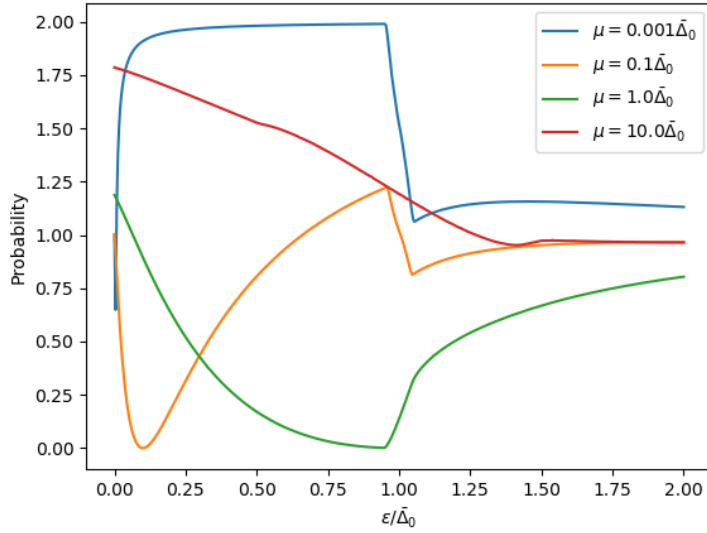
Figure 9: Normalized differential conductance for various values of $\mu_S = \mu_N$ as a function of the energy ε for triplet pairing. When $\varepsilon = \mu < \bar{\Delta}_0$ the conductance goes to zero as there is no hole state to reflect to. Compared to figure 4 with singlet pairing the conductance smoothes around the gap-edge $\varepsilon = \bar{\Delta}_0$. In the sub-gap and supra-gap we see the same behavior as for singlet pairing albeit with a scaled gap.

4   Conclusion

We have studied a TRS preserving WSM where an interface is created between a normal region and a superconducting region by means of the proximity effect or doping. We considered four Weyl nodes, two of each chirality, where the superconducting gap pairs electrons of one branch to the opposite branch in the TRS partner which has the same chirality. We have reproduced the differential current per channel singlet pairing as found by Zhang et al. [1]. Expanding on their research, we have replaced the singlet pairing with the triplet pairing: $\Delta = \Delta_0(p_x + ip_y)/k_F$. The Fermi wavevector is much larger than the linearized momenta allowed in the low energy approximation around the Weyl nodes. As a consequence the location of the Weyl node dominates the amplitude of the gap. As such TRS preserving WSM do not show significantly different behavior for triplet pairing compared to singlet pairing. We suggest further research to repeat the work for a TRS breaking WSM junction with triplet pairing.

References

[1] Song-Bo Zhang, Fabrizio Dolcini, Daniel Breunig, and Björn Trauzettel. Appearance of the universal value e^2/h of the zero-bias conductance in a weyl semimetal-superconductor junction. *Phys. Rev. B*, 97:041116, Jan 2018.

[2] Su-Yang Xu, Ilya Belopolski, Daniel S. Sanchez, Chenglong Zhang, Guoqing Chang, Cheng Guo, Guang Bian, Zhujun Yuan, Hong Lu, Tay-Rong Chang, Pavel P. Shibayev, Mykhailo L. Prokopovych, Nasser Alidoust, Hao Zheng, Chi-Cheng Lee, Shin-Ming Huang, Raman Sankar, Fangcheng Chou, Chuang-Han Hsu, Horng-Tay Jeng, Arun Bansil, Titus Neupert, Vladimir N. Strocov, Hsin Lin, Shuang Jia, and M. Zahid Hasan. Experimental discovery of a topological weyl semimetal state in tap. *Science Advances*, 1(10), 2015.

[3] B. Q. Lv, H. M. Weng, B. B. Fu, X. P. Wang, H. Miao, J. Ma, P. Richard, X. C. Huang, L. X. Zhao, G. F. Chen, Z. Fang, X. Dai, T. Qian, and H. Ding. Experimental Discovery of Weyl Semimetal TaAs. *Physical Review X*, 5(3):031013, Jul 2015.

[4] G. E. Blonder, M. Tinkham, and T. M. Klapwijk. Transition from metallic to tunneling regimes in superconducting microconstrictions: Excess current, charge imbalance, and supercurrent conversion. *Phys. Rev. B*, 25:4515–4532, Apr 1982.

[5] Andreas P. Schnyder and Philip M. R. Brydon. Topological surface states in nodal superconductors. *Journal of Physics Condensed Matter*, 27(24):243201, Jun 2015.

Appendix

Reflection and transmission coefficients

Since only the absolute coefficients are important for calculation of the reflection coefficients we can discard the complex phases ϕ and θ:

$$a_0 = c_0 e^{-i\beta} - d_0 \kappa_{hq},$$
$$-\kappa_h a_0 = c_0 \kappa_{eq} e^{-i\beta} + d_0,$$

Now we can express both a_0 and c_0 in terms of d_0:

$$c_0 = \frac{\kappa_h \kappa_{hq} - 1}{\kappa_{eq} + \kappa_h} e^{i\beta} d_0,$$
$$a_0 = -d_0 \frac{\kappa_{hq} \kappa_{eq} + 1}{\kappa_{eq} + \kappa_h}.$$

The electron-like components require:

$$1 + b_0 \kappa_e = c_0 - \kappa_{hq} e^{-i\beta} d_0,$$
$$\kappa_e + b_0 = c_0 \kappa_{eq} + d_0 e^{-i\beta},$$

equating the two gives an expression for d_0:

$$d_0 = \gamma^{-1} (\kappa_{eq} + \kappa_h)(\kappa_e^2 - 1)$$

with:

$$\gamma = (\kappa_e \kappa_{eq} - 1)(\kappa_h \kappa_{hq} - 1)e^{i\beta} + (\kappa_{hq} + \kappa_e)(\kappa_{eq} + \kappa_h)e^{-i\beta}.$$

From this value of d_0 we express the other coefficients as:

$$a_0 = -\gamma^{-1}(\kappa_e^2 - 1)(\kappa_{hq}\kappa_{eq} + 1),$$
$$b_0 = \gamma^{-1}[e^{i\beta}(\kappa_h \kappa_{hq} - 1)(\kappa_e - \kappa_{eq}) - e^{-i\beta}(\kappa_h + \kappa_{eq})(\kappa_e \kappa_{hq} + 1)],$$
$$c_0 = \gamma^{-1}(\kappa_e^2 - 1)(\kappa_h \kappa_{hq} - 1)e^{i\beta}.$$

The particle group velocity is proportional to the absolute value of the probability current which is proportional to the length of $\mathbf{k}$ which is of the form $\varepsilon \pm \mu_N$ in the normal WSM and $|\Omega \pm \mu_S|$ in the superconducting WSM. Besides the group velocity we also have to take into account the probability current incident to the interface to get the normalization factors:

$$Z_e = \frac{|\varepsilon + \mu_N|}{(1 + |\kappa_e|^2) \cdot |k_e|},$$
$$Z_h = \frac{|\varepsilon - \mu_N|}{(1 + |\kappa_h|^2) \cdot |k_h|},$$
$$Z_{eq} = \left|1 - |e^{-2i\beta}|\right|^{-1} \cdot \frac{|\Omega + \mu_S|}{(1 + |\kappa_{eq}|^2) \cdot |k_{eq}|},$$
$$Z_{hq} = \left|1 - |e^{-2i\beta}|\right|^{-1} \cdot \frac{|\Omega - \mu_S|}{(1 + |\kappa_{hq}|^2) \cdot |k_{hq}|},$$

where we have taken into account the minus sign coming from the holes in the probability current. Since we normalize with respect to the incoming electron the reflection/transmission constants are: $R_{eh} = |a_0|^2 \cdot Z_e/Z_h$, $R_{ee} = |b_0|^2$, $T_{ee} = |c_0|^2 \cdot Z_e/Z_{eq}$ and $T_{eh} = |d_0|^2 \cdot Z_e/Z_{hq}$.